Part A for ScholarWorks@UA collection
Moment tensors for the mainshock and aftershocks of the 2018-11-30 M_w 7.1 Anchorage earthquake

Cole Richards and Carl Tape

Version 1: May 15, 2019
Version 2: August 15, 2019

Attribution: If you use these files, please cite *Richards* (2019) and *West et al.* (2019) or *Ruppert et al.* (2019). This document is downloadable as a pdf via the link listed in *Richards* (2019). This is Part A of the collection; see also Part B, which focuses on the mainshock.

Overview: This collection contains results from estimating moment tensor solutions for the 2018-11-30 M_w 7.1 Anchorage earthquake and 18 of its aftershocks. The first 10 are used by *West et al.* (2019) and the complete 18 are used by *Ruppert et al.* (2019). Figure A1 provides an overview of the tectonic setting.

Description of files

A summary of files in the collection is listed in the following table:

file name	description
scholarworks_ashock.pdf	this file: summary of collection, including seismicity map, beachball and subset of waveform fits for one aftershock
waveform_fits_ashock.pdf	catalog of all 18 aftershock waveform fits
beachballs_ashock.pdf	catalog of all 18 aftershock best-fitting moment tensors (beachballs)
anchorage_ashock_mech.txt	text file catalog of moment tensors
weight_ashock.zip	zipped set of text files of input parameters for moment tensor inversions with all stations

Event selection

We selected events from the catalog of *West et al.* (2019), which was produced by Natalia Ruppert using hypoDD. This catalog of 674 events was provided to us on 2019-01-11 and includes events that occurred between 2018-11-13 and 2019-01-01. It includes all reviewed events $M_l \geq 2.5$ through December 9 and $M_l \geq 3.5$ through end of December. From this catalog we selected all events $M_l \geq 4.2$ starting 2018-12-01. The aftershock region that we searched is defined as -149.8–-150.1 E longitude and 61.2–61.5 N latitude. This resulted in 11 aftershocks.

One of the 11 events (2018-12-01 07:07:29.710, M_l 4.3) occurred 8 seconds prior to a larger (M_l 5.0) event. The waveforms for the larger event masked out those from the smaller event, and therefore we excluded the smaller event, leaving 10 for our initial analysis.

This manuscript was later updated to include a second set of aftershocks from 2019-01-01–2019-06-01 with $M_l \geq 4.0$ for the same region. This produced 8 additional aftershocks. The

updated catalog of 18 aftershocks is a contribution to *Ruppert et al.* (2019).

Waveform fits: Figure A4 and [`waveform_fits_ashock.pdf`]

Waveform fits for 18 moment tensor inversions for which waveform misfit is plotted on the source-type plot. Black are observed waveforms; red are synthetic waveforms computed using a frequency-wavenumber method (*Zhu and Rivera*, 2002) that assumes a (1D) layered model. The waveforms are fit separately within five time windows: P wave vertical component (PV), P wave radial component (PR), Rayleigh wave vertical component (SurfV), Rayleigh wave horizontal component (SurfR), and Love wave transverse component (SurfT). At far left in each row is the station name, source-station distance in km, and station azimuth in degrees. Below each pair of waveforms are four numbers: the cross-correlation time shift between data and synthetics, the cross-correlation value, the percent of the misfit function represented by the waveform pair, and the amplitude ratio between waveforms, $\ln(A_{\rm obs}/A_{\rm syn})$, where A is the max value of the waveform within the time window.

The beachball represents the best solution M_0 (i.e., the global minimum of the misfit function). The beachball is plotted as a lower-hemisphere projection (standard seismological convention) of the moment tensor. The surrounding black dots denote the azimuthal location of the stations used, and the red crosses denote the lower hemisphere piercing points of the ray paths to the stations.

Here is a header for an example event in Figure A4:

```
Event 20181201053153980 Model scak Depth 46
FM 175 58.643581 -70 Mw 4.50 γ 0 δ 0 rms 3.910e-01 VR 89.8 pol_wt 999.00
Filter periods (seconds): Body:1.50-4.00. Surf:16.00-40.00 duration: 1.00/0.50 s
# norm L1 # Pwin 15 Swin 150 # N 67 Np 81 Ns 154
```

The four header lines are as follows:

1. `Event 20181201053153980 Model scak Depth 46`
   The event ID is derived from the origin time of 2018-12-01 05:31:53.980
   The layered model used is `scak`, and the event depth is 46 km.

2. `FM 175 58.643581 -70 Mw 4.50 γ 0 δ 0 rms 3.910e-01 VR 89.8 pol_wt 999.00`
   The orientation of the moment tensor solution M_0 is strike 175°, dip 58°, rake −70°. The estimated magnitude is $M_{\rm w}$ 4.50. The source type of M_0 is expressed in terms of lune longitude $\gamma = 0°$ and lune latitude $\delta = 0°$. (For the aftershocks we assume the double couple constraint.) The waveform difference between data and synthetics is $RMS = 0.3910$, and the variance reduction is $VR = 89.8\%$. These are based on a waveform difference measure that rewards using longer time windows and broader bandpass limits. This choice means that the VR cannot be directly compared with VR values reported in other studies.

   If polarities are used in the misfit function, then the factor `pol_wt` determines the balance between fitting waveforms and fitting polarities. A value of 999.0 means that polarities are not used.

3. `Filter periods (seconds): Body:1.50-4. Surf:16-40 duration: 1.00/0.50 s`
   The body waves, if used the inversions, were filtered 1.50–4 s, the surface waves were filtered 16–40 s.
   The source time function is a trapezoidal function whose duration is 1.00 s and whose rise time is half the duration. The duration is not an estimated source parameter but is set according to the target frequency of body waveforms (here 0.25–0.667 Hz).

4. `# norm L1 # Pwin 15 Swin 150 # N 67 Np 81 Ns 154`
   An L1 norm was used for the misfit function (e.g., *Silwal and Tape*, 2016). The (reference) P-window is 15 s long and the surface wave window is 150 s long. There are 67 stations (N), 81 P wave windows (Np), and 154 surface wave windows (Ns).

The numbers below each station are

1. source–station epicentral distance, km
2. station azimuth, in degrees
3. time shift between picked P onset and synthetic P onset.
4. sign of the observed first-motion polarity, which is either 1 (up or compression) or -1 (down or dilatation). The number in parentheses is the predicted amplitude, which ranges between $\pm\sqrt{2}$; numbers close to zero indicate that the station is near a nodal surface of the radiation pattern for the assumed mechanism.

The four numbers below each pair of waveforms are

1. the cross-correlation time shift $\Delta T = T_{\rm obs} - T_{\rm syn}$ required for matching the synthetics $s(t)$ with the data $u(t)$. A positive time-shift means that the synthetics arrive earlier than the data and that the assumed velocity model is faster than the actual earth structure.
2. the maximum cross-correlation percentage between $u(t)$ and $s(t - \Delta T)$
3. the percentage of the total misfit
4. the amplitude ratio $\ln(A_{\rm obs}/A_{\rm syn})$ in each time window

Best-fitting moment tensors: Figure A5 and [`beachballs_ashock.pdf`]

Best-fitting moment tensors for 18 aftershocks of the 2018-11-30 $M_{\rm w}$ 7.1 Anchorage earthquake. X symbols show the lower-hemisphere piercing points of the ray paths to each station used in the moment tensor search. The text labels on the outside denote the station directions (azimuths) relative to the source. The magnitudes are obtained using an increment of $\Delta M_{\rm w} = 0.05$, with the depth fixed to relocated hypocenters (*West et al.*, 2019)(*Ruppert et al.*, 2019).

Text file table for moment tensor catalog [`anchorage_ashock_mech.txt`]

Seismic moment tensor catalog of 18 events. Details can be found within the header lines, which also refer to *Kanamori* (1977); *Silver and Jordan* (1982); *Tape and Tape* (2012).

Input text files used in the moment tensor inversion [`weight_ashock.zip`]

We provide a text file for each of the 18 events in this study. These files show which stations and which time windows were used (or not) in each moment tensor inversion.

References

Bird, P. (2003), An updated digital model of plate boundaries, *Geochem. Geophy. Geosyst.*, *4*, 1027, doi:10.1029/2001GC000252.

Eberhart-Phillips, D., D. H. Christensen, T. M. Brocher, R. Hansen, N. A. Ruppert, P. J. Haeussler, and G. A. Abers (2006), Imaging the transition from Aleutian subduction to Yakutat collision in central Alaska, with local earthquakes and active source data, *J. Geophys. Res.*, *111*, B11303, doi:10.1029/2005JB004240.

Ekström, G., M. Nettles, and A. M. Dziewoński (2012), The global GCMT project 2004–2010: Centroid-moment tensors for 13,017 earthquakes, *Phys. Earth Planet. Inter.*, *200-201*, 1–9, doi:10.1016/j.pepi.2012.04.002.

Fu, Y., and J. T. Freymueller (2013), Repeated large Slow Slip Events at the south central Alaska subduction zone, *Earth Planet. Sci. Lett.*, *375*, 303–311.

Haeussler, P. J., R. W. Saltus, R. G. Stanley, N. Ruppert, K. Lewis, S. M. Karl, and A. Bender (2017), The Peters Hills basin, a Neogene wedge-top basin on the Broad Pass thrust fault, south-central Alaska, *Geosphere*, *13*(5), 1464–1488, doi:10.1130/GES01487.1.

Hayes, G. P., G. L. Moore, D. E. Portner, M. Hearne, H. Flamme, M. Furtney, and G. M. Smoczyk (2018), Slab2, a comprehensive subduction zone geomety model, *Science*, doi:10.1126/science.aat4723.

Kanamori, H. (1977), The energy release in great earthquakes, *J. Geophys. Res.*, *82*, 2981–2987.

Kirschner, C. E. (1988), Map Showing Sedimentary Basins of Onshore and Continental Shelf Areas, Alaska, U.S. Geol. Survey Miscellaneous Investigation Series I-1873.

Koehler, R. D., R.-E. Farrell, P. A. C. Burns, and R. A. Combellick (2012), Quaternary faults and folds in Alaska: A digital database, doi:10.14509/23944, Alaska Div. Geol. Geophys. Surv. Miscellaneous Publication 141, 31 p., 1 sheet, scale 1:3,700,000.

Li, S., J. Freymueller, and R. McCaffrey (2016), Slow slip events and time-dependent variations in locking beneath Lower Cook Inlet of the Alaska-Aleutian subduction zone, *J. Geophys. Res. Solid Earth*, *121*, 1060–1079, doi:10.1002/2015JB012491.

Ohta, Y., J. T. Freymueller, S. Hreinsdóttir, and H. Suito (2006), A large slow slip event and the depth of the seismogenic zone in the south central Alaska subduction zone, *Earth Planet. Sci. Lett.*, *247*, 108–116.

Richards, C. (2019), Moment tensors for the mainshock and aftershocks of the 2018-11-30 M_w 7.1 Anchorage earthquake, ScholarWorks@UA at `http://hdl.handle.net/11122/10173` (last accessed 2019-05-16): descriptor files, text file of catalog, and figures of waveform fits.

Ruppert, N. A., A. Nayak, C. Thurber, and C. Richards (2019), Aftershock analysis of the 2018 Mw 7.1 Anchorage, Alaska, earthquake: Relocations and regional moment tensors, *Seismol. Res. Lett.* (in review).

Shah, A. K., R. G. Stanley, K. Lewis, P. J. Haeussler, C. J. Potter, R. W. Saltus, and J. D. Phillips (2015), Aeromagnetic survey data used to map features of the Cook Inlet and Susitna basins, Alaska, Abstract presented at 2015 AGU-SEG Workshop, Denver, Colo., 25-27 Aug.

Shellenbaum, D. P., L. S. Gregersen, and P. R. Delaney (2010), Top Mesozoic unconformity depth map of the Cook Inlet Basin, Alaska, doi:10.14509/21961, Alaska Div. Geol. Geophys. Surv. Report of Investigation 2010-2, 1 sheet, scale 1:500,000, available at `http://www.dggs.alaska.gov/pubs/id/21961` (last accessed 2016-10-30).

Silver, P. G., and T. H. Jordan (1982), Optimal estimation of scalar seismic moment, *Geophys. J. R. Astron. Soc.*, *70*, 755–787.

Silwal, V., and C. Tape (2016), Seismic moment tensors and estimated uncertainties in southern Alaska, *J. Geophys. Res. Solid Earth*, *121*, 2772–2797, doi:10.1002/2015JB012588.

Silwal, V., C. Tape, and A. Lomax (2018), Crustal earthquakes in the Cook Inlet and Susitna region of southern Alaska, *Tectonophysics*, *745*, 245–263, doi:10.1016/j.tecto.2018.08.013.

Tape, W., and C. Tape (2012), A geometric setting for moment tensors, *Geophys. J. Int.*, *190*, 476–498, doi:10.1111/j.1365-246X.2012.05491.x.

Wei, M., J. J. McGuire, and E. Richardson (2012), A slow slip event in the south central Alaska Subduction Zone and related seismicity anomaly, *Geophys. Res. Lett.*, *39*, L15309, doi:10.1029/2012GL052351.

West, M. E., A. Bender, M. Gardine, L. Gardine, K. Gately, P. Haeussler, W. Hassan, F. Meyer, C. Richards, C. Tape, J. Thornley, and R. Witter (2019), The 30 November 2018 Mw 7.1 Anchorage earthquake, *Seismol. Res. Lett.* (in review).

Zhu, L., and L. A. Rivera (2002), A note on the dynamic and static displacements from a point source in multilayered media, *Geophys. J. Int.*, *148*, 619–627, doi:10.1046/j.1365-246X.2002.01610.x.

Table A1: Fault parameters for 18 estimated moment tensors (see also Figure A2). The average dip of the first fault plane is 63.4°. The average dip of the second fault plane is 31.7°.

otime	longitude	latitude	depth	M_w	strike1	dip1	rake1	strike2	dip2	rake2
2018-12-01 05:31:53	-150.0083	61.3780	46.3	4.50	174.8	58.6	-69.9	319.7	36.7	-119.4
2018-12-01 07:07:37	-149.9479	61.4850	48.3	4.90	200.6	75.0	-68.9	324.6	25.7	-143.2
2018-12-01 07:57:22	-150.0082	61.3654	46.2	5.00	190.7	54.1	-74.8	345.9	38.5	-109.9
2018-12-01 12:44:53	-149.9064	61.4858	41.4	4.50	185.5	57.5	-89.4	4.4	32.5	-91.0
2018-12-02 04:52:14	-150.0022	61.3548	46.8	4.45	193.6	73.1	-71.2	324.1	25.1	-136.7
2018-12-04 16:02:29	-150.0931	61.4087	42.7	4.55	184.3	61.3	-68.2	324.4	35.5	-124.2
2018-12-05 12:48:44	-150.0823	61.3439	46.0	4.50	175.2	66.0	-88.8	352.3	24.0	-92.6
2018-12-06 21:45:11	-150.0107	61.3502	44.9	4.65	188.6	64.2	-81.1	348.8	27.2	-107.7
2018-12-09 19:00:32	-149.8831	61.4494	39.9	4.65	169.4	62.8	-87.9	344.9	27.2	-94.0
2018-12-27 14:21:13	-150.1164	61.3034	46.0	4.80	185.4	72.0	-70.6	316.5	26.2	-135.7
2019-01-01 03:03:30	-149.9028	61.3006	44.7	4.90	175.5	55.3	-107.4	24.3	38.3	-66.7
2019-01-02 15:16:03	-149.9208	61.3078	46.2	4.25	179.4	61.3	-90.4	0.2	28.7	-89.3
2019-01-11 02:33:38	-149.8991	61.4708	49.8	4.55	161.2	75.0	-66.2	281.6	27.9	-146.5
2019-01-23 05:41:48	-150.2064	61.4806	48.4	4.55	206.6	61.5	-89.2	24.9	28.5	-91.5
2019-02-06 20:04:45	-149.9644	61.3953	47.1	4.20	209.7	75.9	-63.4	325.7	29.9	-150.7
2019-02-18 17:02:46	-149.9256	61.4574	40.9	4.45	195.5	60.4	-95.5	26.4	30.1	-80.5
2019-03-23 15:14:45	-149.8616	61.5263	47.4	4.20	223.8	51.9	-58.5	359.0	47.8	-123.7
2019-05-19 07:01:53	-149.9555	61.3203	46.3	4.10	203.8	54.9	-65.7	345.7	41.8	-120.3

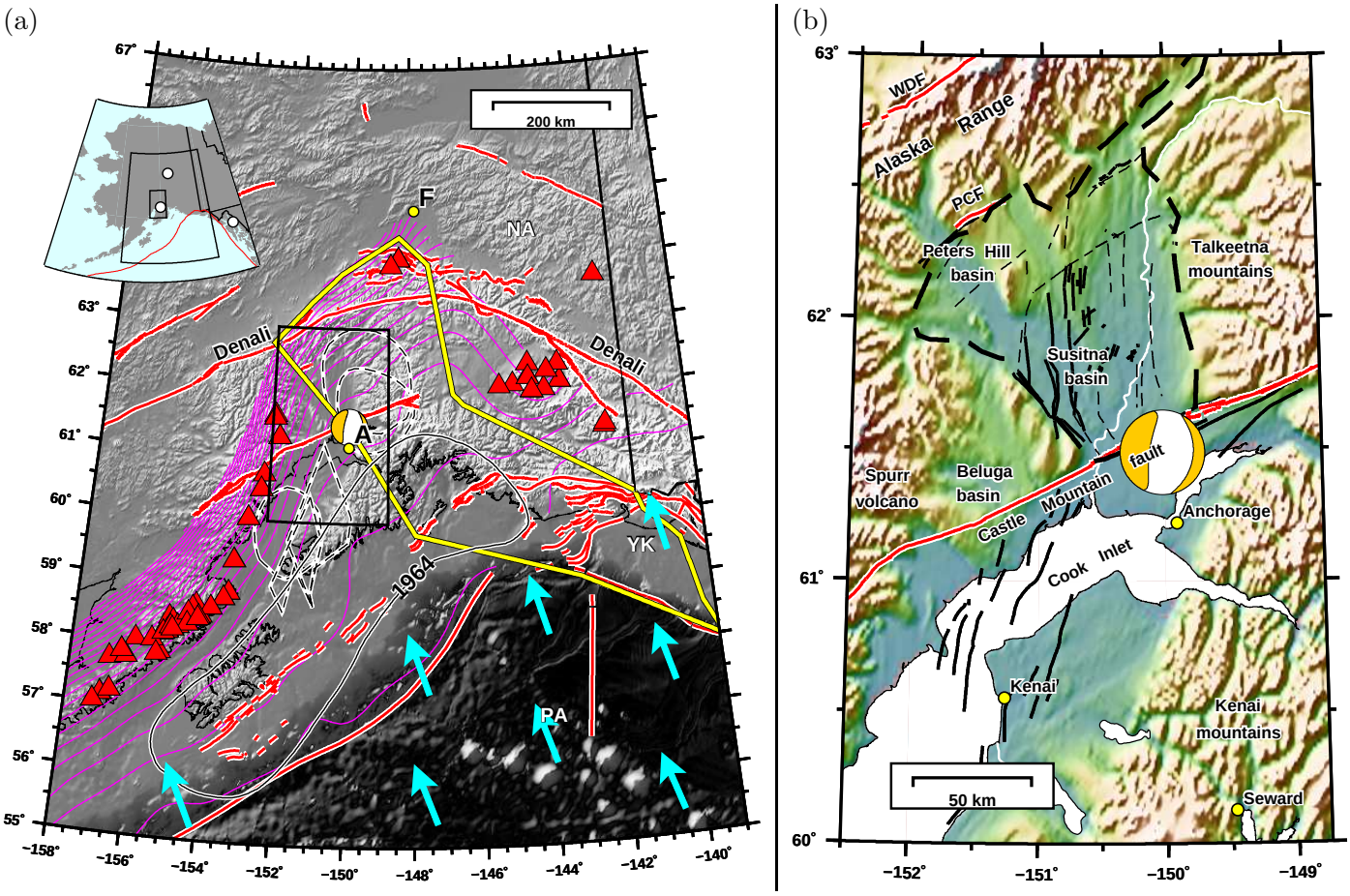

Figure A1: Adapted from Figure 1 of *Silwal et al.* (2018). The beachball plotted is the GCMT solution (*Ekström et al.*, 2012) for the 2018-11-30 M_w 7.1 Anchorage earthquake (depth 48.2 km). (a) Active tectonic setting of the Aleutian–Alaskan subduction zone, south-central Alaska. The rectangle in the middle shows the main study region. Cyan arrows shows the plate vectors for the subducting Pacific plate (PA) under the North American plate (NA) (*Bird*, 2003). Red lines denote active faults (*Koehler et al.*, 2012). Magenta curves are the contours of the subduction interface, i.e.,, the top of the Pacific plate (*Hayes et al.*, 2018). Yellow bounded region denotes the surface and subsurface extent of the Yakutat block (YK) (*Eberhart-Phillips et al.*, 2006). Red triangles represent active volcanoes. Black dashed lines are inferred slow slip events from various sources (*Ohta et al.*, 2006; *Wei et al.*, 2012; *Fu and Freymueller*, 2013; *Li et al.*, 2016). Also marked is the aftershock zone of the 1964 M_w 9.2 earthquake. Labeled cities: Anchorage (A) and Fairbanks (F). (b) Physiographic map of the Cook Inlet and Susitna region, south-central Alaska. Active faults are plotted in red and include Castle Mountain, Pass Creek (PCF), and the western Denali fault (WDF) at upper left (*Koehler et al.*, 2012). Cook Inlet sedimentary basin underlies Cook Inlet and the western Kenai peninsula (*Shellenbaum et al.*, 2010). North of the Castle Mountain fault are three sedimentary basins: Beluga, Susitna, and Peters Hill. Active folds in Cook Inlet basin (*Koehler et al.*, 2012) are marked in black. Other faults in Susitna basin also marked in black are obtained from *Haeussler et al.* (2017); *Shah et al.* (2015). The thick black dashed line denotes the boundary of Susitna lowlands *Kirschner* (1988).

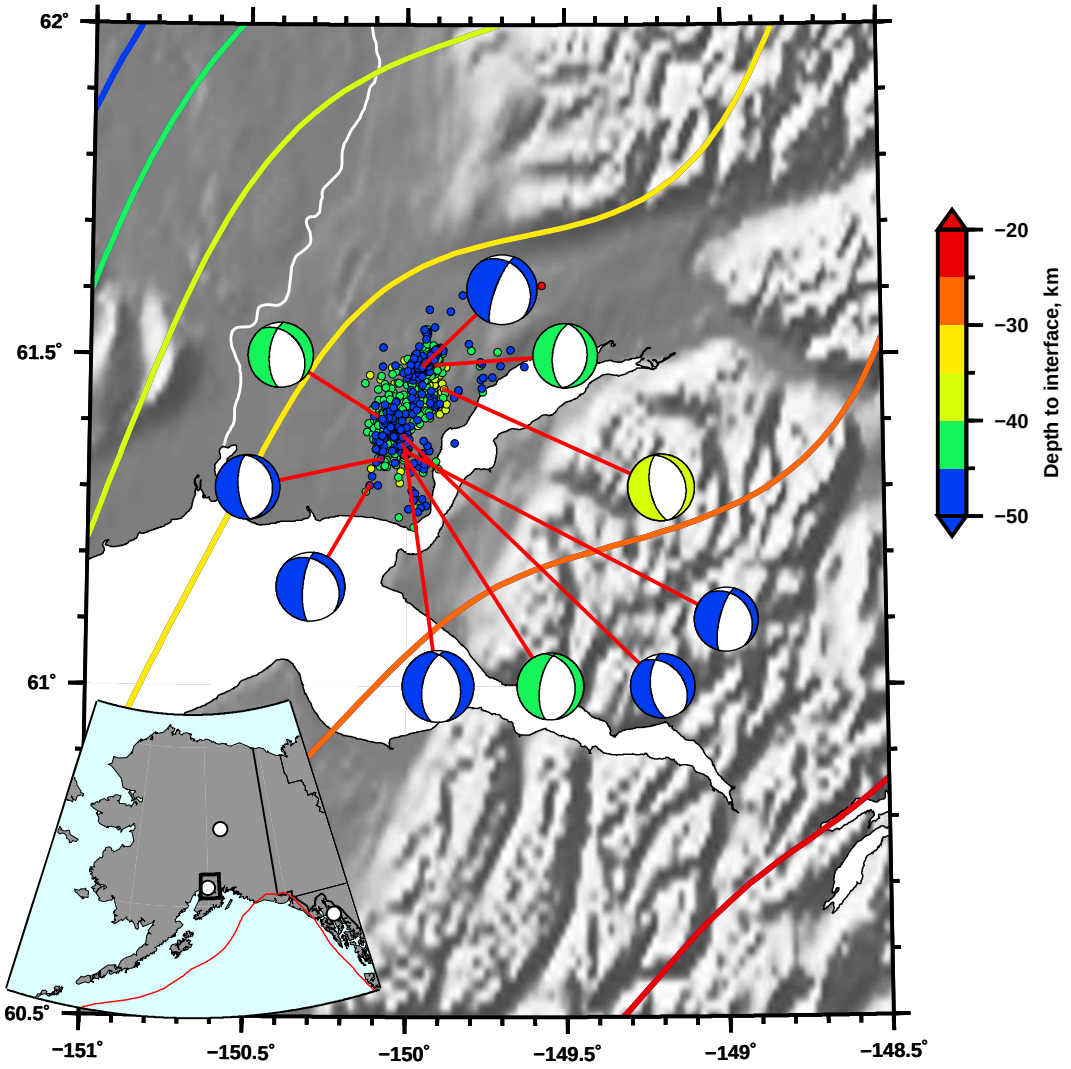

Figure A2: Moment tensors for 10 aftershocks of the 2018-11-30 M_w 7.1 Anchorage earthquake (Table A1). The contours of the subduction interface (*Hayes et al.*, 2018) are for 25, 30, 35, 40, 45, and 50 km. Small circles are relocated aftershocks (*West et al.*, 2019). The beachballs and relocated aftershocks are colored by depth. The subduction interface is at approximately 33 km depth where it overlies the source region of the M_w 7.1 earthquake.

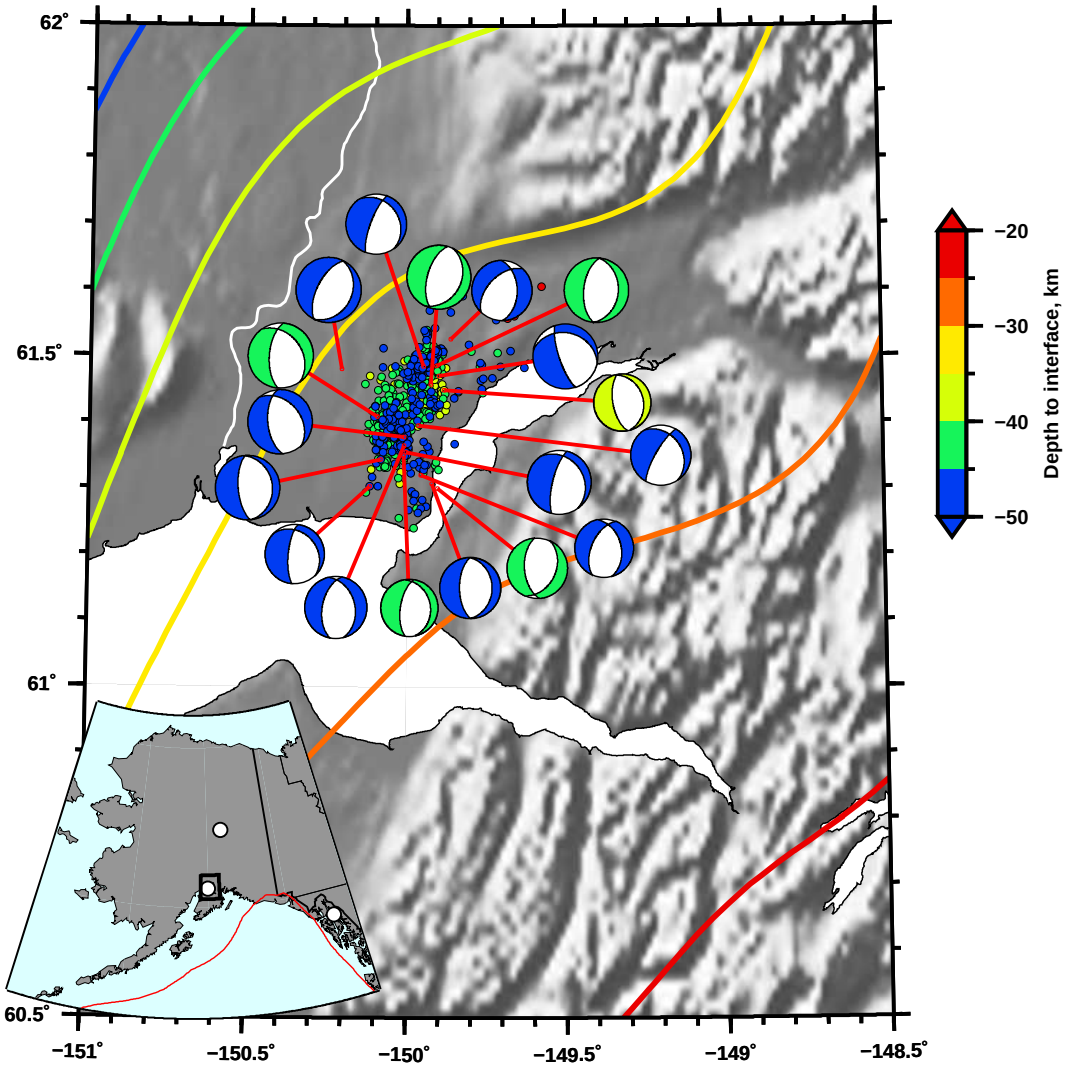

Figure A3: Moment tensors for 18 aftershocks (including the 10 from Figure A2) of the 2018-11-30 M_{w} 7.1 Anchorage earthquake (Table A1). The contours of the subduction interface (*Hayes et al.*, 2018) are for 25, 30, 35, 40, 45, and 50 km. Small circles are relocated aftershocks (*West et al.*, 2019). The beachballs and relocated aftershocks are colored by depth. The subduction interface is at approximately 33 km depth where it overlies the source region of the M_{w} 7.1 earthquake.

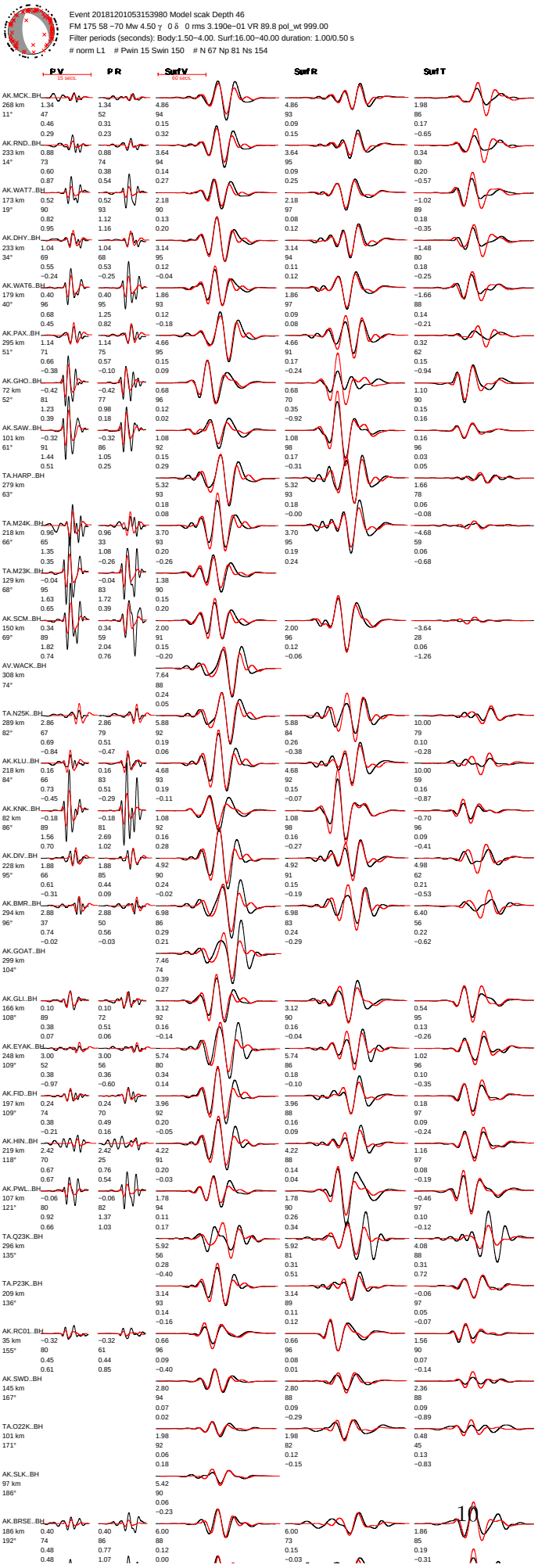

Figure A4: Best-fitting moment tensor and waveform fits for event 20181201053153980. Red = time-shifted synthetics, black = data. For each station, the five time windows are for P wave vertical (PV), P wave radial (PR), Rayleigh waves (Surf V, Surf R), and Love waves (Surf T). Numbers beneath each waveform pair are the time shift, the cross correlation maximum, the percentage of the misfit function, and the log amplitude ratio. The stations are sorted by azimuth from 0–360 degrees (relative to the source).

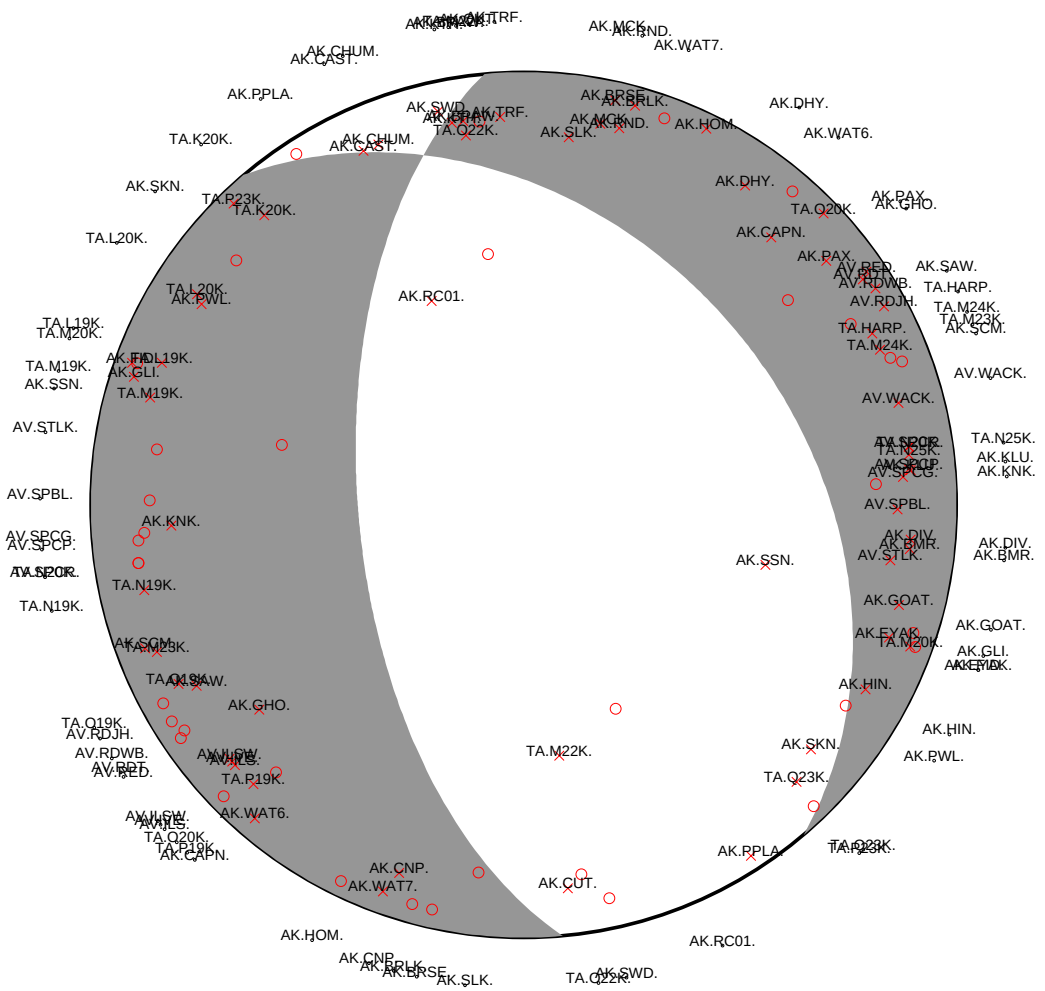

Figure A5: Best-fitting moment tensor for a M_w 4.50 aftershock of the 2018-11-30 M_w 7.1 Anchorage earthquake. X symbols show the lower-hemisphere piercing points of the ray paths to each station used in the moment tensor search. The text labels on the outside denote the station directions (azimuths) relative to the source. The magnitude is obtained using an increment of $\Delta M_w = 0.05$, with the depth fixed to a relocated hypocenter (*West et al.*, 2019). Figure A4 and [`waveform_fits_ashock.pdf`] display the waveform fits for this aftershock.